Eur. Phys. J. A **7**, 127–137 (2000)

THE EUROPEAN PHYSICAL JOURNAL A

EDP Sciences

Subthreshold and near threshold K^+ meson photoproduction on nuclei

E.Ya. Paryev

Institute for Nuclear Research, Russian Academy of Sciences, Moscow 117312, Russia

Received: 12 April 1999 / Revised version: 11 September 1999
Communicated by W. Weise

Abstract. The inclusive K^+ meson production in photon–induced reactions in the near threshold and subthreshold energy regimes is analyzed with respect to the one–step ($\gamma N \to K^+ Y$, $Y = \Lambda, \Sigma$) incoherent production processes on the basis of an appropriate new folding model, which takes properly into account the struck target nucleon removal energy and internal momentum distribution (nucleon spectral function), extracted from recent quasielastic electron scattering experiments and from many–body calculations with realistic models of the NN interaction. Simple parametrizations for the total and differential cross sections of the K^+ production in photon–nucleon collisions are presented. Comparison of the model calculations of the K^+ differential cross sections for the reaction $\gamma + C^{12}$ in the threshold region with the existing experimental data is given, that displays the contributions to the K^+ production at considered incident energies coming from the use of the single–particle part as well as high momentum and high removal energy part of the nucleon spectral function. Detailed predictions for the K^+ total and differential cross sections from γH^2, γC^{12} and γPb^{208} reactions at subthreshold and near threshold energies are provided. The influence of the uncertainties in the elementary K^+ production cross sections on the K^+ yield is explored.

PACS. 25.20.Lj Photoproduction reactions – 21.80.+a Hypernuclei

1 Introduction

An extensive investigations of the production of K^+ mesons in proton–nucleus reactions [1–15] at incident energies lower than the free nucleon-nucleon threshold have been carried out over the last years. Because of rather weak K^+ rescattering in the surrounding medium compared to pions, etas, antiprotons and antikaons, one hopes to extract from these studies information about both the intrinsic properties of target nuclei (such as Fermi motion, high–momentum components of the nuclear wave function, clusters of nucleons or quarks) and reaction mechanism, in–medium properties of hadrons. There are essentially less extensive investigations [16, 17] of the inclusive subthreshold kaon production in pion–nucleus reactions. Finally, the electromagnetic production of K^+ mesons on nuclei in the threshold region has up to now received very little consideration [18], probably, because of a lack of suitable facilities and associated detectors. Since the cross sections of (γ, K^+) reaction at subthreshold and near threshold energies are expected to be extremely small (about one hundred times smaller than those of (π^+, K^+) reaction in the same kinematical conditions), high duty cycle and high intensity electron beams are needed to allow accurate inclusive (γ, K^+) measurements on nuclear targets in the threshold region. Such measurements are planned to be conducted in the near future at the Continuous Electron Beam Accelerator Facility (CEBAF) [19, 20] using the tagged photon beam in the CLAS (the CEBAF Large Acceptance Spectrometer) detector system. New data from CEBAF [19, 20] will hopefully permit improving our understanding of the phenomenon of the near threshold and subthreshold kaon production in composite hadronic systems, since we can take here advantage of the much cleaner electromagnetic probes, compared to hadronic ones. It is clear that, in order to analyze such data, a relevant formalism has to be developed.

The main goal of the present work is to extend the spectral function approach [10] that has been employed by us for the description of the measured total [1] and differential [8] kaon production cross sections from pC^{12} collisions in the near threshold and subthreshold energy regimes to K^+–producing electromagnetic processes. It is evident that the use of a single model to describe simultaneously K^+ production on nuclei in the threshold region from hadronic and electromagnetic probes will enable us to disentangle reliably the underlying reaction mechanism. In this paper we present the detailed predictions for the K^+ total and differential cross sections from $\gamma + H^2$, $\gamma + C^{12}$ and $\gamma + Pb^{208}$ reactions in the threshold energy region obtained in the framework of the first collision model

[10] based on nucleon spectral function and compare part of them with the available data.

2 First collision model

An incident photon can produce a K^+ directly in the first inelastic γN collision due to nucleon Fermi motion. Since we are interested in the bombarding energy region up to approximately 1.4 GeV, we have taken into account the following elementary processes which have the lowest free production thresholds (respectively, 0.911, 1.046 and 1.052 GeV) [1] :

$$\gamma + p \to K^+ + \Lambda, \tag{1}$$

$$\gamma + p \to K^+ + \Sigma^0, \tag{2}$$

$$\gamma + n \to K^+ + \Sigma^-. \tag{3}$$

Because the mean–free paths both of γ and K^+ in the nuclear medium are relatively long compared to those of p, $\pi^{\pm}$ and K^- due to the small photon–nucleon and kaon–nucleon cross sections, we will neglect the photon initial– and kaon final–state interactions in the present study. Moreover, since the kaon mass in the medium is approximately not affected by medium effects [21] as well as in view of the substantial uncertainties of the model hyperon self–energies [22–24], we will also ignore the medium modification of hadron masses in the present work. Then we can represent the invariant inclusive cross section of K^+ production on nuclei by the initial photon with momentum $\mathbf{p}_\gamma$ as follows [10]:

$$E_{K^+}\frac{d\sigma^{(prim)}_{\gamma A\to K^+X}(\mathbf{p}_\gamma)}{d\mathbf{p}_{K^+}} = Z\left[\left\langle E_{K^+}\frac{d\sigma_{\gamma p\to K^+\Lambda}(\mathbf{p}_\gamma,\mathbf{p}_{K^+})}{d\mathbf{p}_{K^+}}\right\rangle + \left\langle E_{K^+}\frac{d\sigma_{\gamma p\to K^+\Sigma^0}(\mathbf{p}_\gamma,\mathbf{p}_{K^+})}{d\mathbf{p}_{K^+}}\right\rangle\right] + N\left\langle E_{K^+}\frac{d\sigma_{\gamma n\to K^+\Sigma^-}(\mathbf{p}_\gamma,\mathbf{p}_{K^+})}{d\mathbf{p}_{K^+}}\right\rangle, \tag{4}$$

where

$$\left\langle E_{K^+}\frac{d\sigma_{\gamma N\to K^+Y}(\mathbf{p}_\gamma,\mathbf{p}_{K^+})}{d\mathbf{p}_{K^+}}\right\rangle = \iint P(\mathbf{p}_t,E)d\mathbf{p}_t dE \times\left[E_{K^+}\frac{d\sigma_{\gamma N\to K^+Y}(\sqrt{s},\mathbf{p}_{K^+})}{d\mathbf{p}_{K^+}}\right]. \tag{5}$$

Here, $E_{K^+}d\sigma_{\gamma N\to K^+Y}(\sqrt{s},\mathbf{p}_{K^+})/d\mathbf{p}_{K^+}$ are the free invariant inclusive cross sections for K^+ production in reactions (1)–(3); $P(\mathbf{p}_t,E)$ is the nucleon spectral function normalized to unity; $\mathbf{p}_t$ and E are the internal momentum and removal energy of the struck target nucleon just before the collision; Z and N are the numbers of protons and neutrons in the target nucleus (A=N+Z); $\mathbf{p}_{K^+}$ and E_{K^+} are the momentum and total energy of the K^+ meson, respectively; $E_{K^+}=\sqrt{p^2_{K^+}+m^2_K}$ (m_K is the rest mass of a kaon in free space); s is the γN center–of–mass energy squared. The expression for s is:

$$s=(E_\gamma+E_t)^2-(\mathbf{p}_\gamma+\mathbf{p}_t)^2, \tag{6}$$

where E_γ and E_t are the projectile total energy, given by $E_\gamma=p_\gamma$, and the struck target nucleon total energy, respectively. Taking into account the recoil and excitation energies of the residual $(A-1)$ system, one has [10, 25]:

$$E_t=M_A-\sqrt{(-\mathbf{p}_t)^2+(M_A-m_N+E)^2}, \tag{7}$$

where M_A and m_N are the rest masses of the initial target nucleus and nucleon. It is easily seen that in this case the struck target nucleon is off–shell. In (4) any difference between the proton and the neutron spectral functions is disregarded [10].

Taking into consideration the two–body kinematics of the elementary processes (1)-(3), we can readily get the following expressions for the Lorentz invariant inclusive cross sections for these processes:

$$E_{K^+}\frac{d\sigma_{\gamma N\to K^+Y}(\sqrt{s},\mathbf{p}_{K^+})}{d\mathbf{p}_{K^+}} = \frac{\pi}{I_2(s,m_Y,m_K)}\frac{d\sigma_{\gamma N\to K^+Y}(s)}{d\overset{*}{\mathbf{\Omega}}} \times\frac{1}{(\omega+E_t)}\delta\left[\omega+E_t-\sqrt{m_Y^2+(\mathbf{Q}+\mathbf{p}_t)^2}\right], \tag{8}$$

where

$$I_2(s,m_Y,m_K)=\frac{\pi}{2}\frac{\lambda(s,m_Y^2,m_K^2)}{s}, \tag{9}$$

$$\lambda(x,y,z)=\sqrt{\left[x-(\sqrt{y}+\sqrt{z})^2\right]\left[x-(\sqrt{y}-\sqrt{z})^2\right]}, \tag{10}$$

$$\omega=E_\gamma-E_{K^+},\ \mathbf{Q}=\mathbf{p}_\gamma-\mathbf{p}_{K^+}. \tag{11}$$

Here, $d\sigma_{\gamma N\to K^+Y}(s)/d\overset{*}{\mathbf{\Omega}}$ are the K^+ differential cross sections in the γN center–of–mass system normalized to the corresponding total experimental cross sections $\sigma_{\gamma N\to K^+Y}$; m_Y is the mass in free space of a Y hyperon (Λ or Σ). The existing experimental data (see Figs. 1–3) on the total cross sections $\sigma_{\gamma N\to K^+Y}$ have been fitted (see, also, Figs. 1–3) by the following simple expressions:

$$\sigma_{\gamma N\to K^+Y}(\sqrt{s})=\frac{A_Y(\sqrt{s}-\sqrt{s_0})}{B_Y+(\sqrt{s}-\sqrt{s_0})^2}, \tag{12}$$

$$\sigma_{\gamma p\to K^+\Sigma^0}(\sqrt{s}) = \begin{cases} 8.67\left(\frac{\sqrt{s}-\sqrt{\tilde{s}_0}}{\mathrm{GeV}}\right)^{0.7907}\ [\mu\mathrm{b}] & \text{for } \sqrt{\tilde{s}_0}<\sqrt{s}\le 1.873\,\mathrm{GeV} \\ 0.3665\left(\frac{\mathrm{GeV}}{\sqrt{s}-\sqrt{\tilde{s}_0}}\right)^{1.0956}\ [\mu\mathrm{b}] & \text{for } \sqrt{s}>1.873\,\mathrm{GeV}, \end{cases} \tag{13}$$

[1] We can neglect in the energy domain of our interest the K^+ production processes with higher kaon ($K^+(892)$) and hyperon ($\Lambda(1405)$, $\Lambda(1520)$, $\Sigma^0(1385)$) resonances in the final states due to their larger production thresholds in γN collisions. For example, the threshold for free $\Sigma^0(1385)$ excitation is 1.412 GeV.

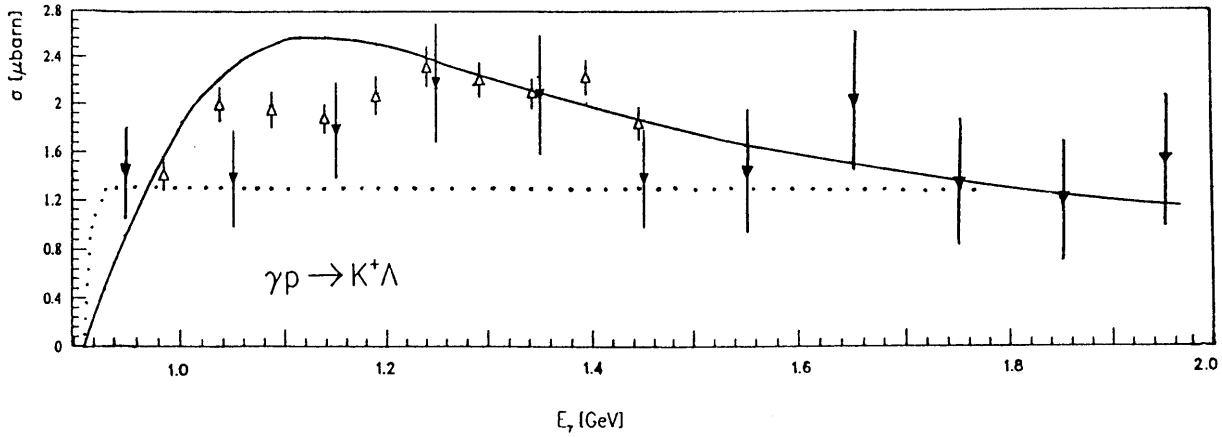

Fig. 1. Total cross section for the reaction $\gamma p \to K^+\Lambda$ as a function of photon energy. The solid and dotted lines are calculations by (12) and (16), respectively. Data are from [26] (open triangles), and [27] (full triangles)

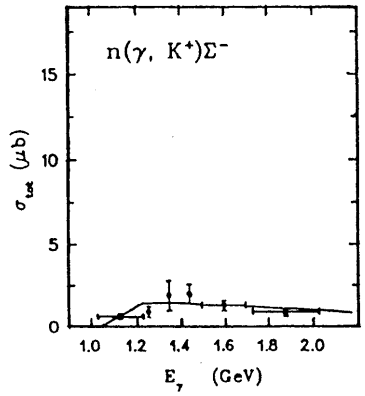

Fig. 2. Total cross section for the reaction $\gamma n \to K^+\Sigma^-$ as a function of photon energy. The solid line is calculation by (12). Data are from [28]

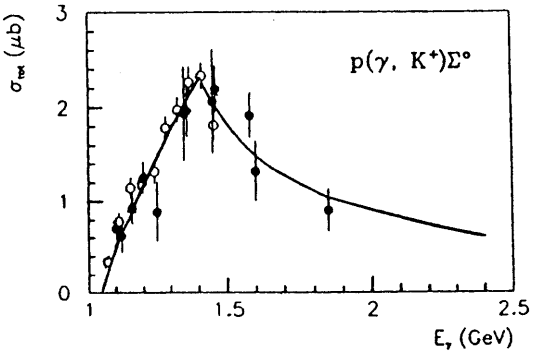

Fig. 3. Total cross section for the reaction $\gamma p \to K^+\Sigma^0$ as a function of photon energy. The solid line is calculation by (13). Data are from [26] (open circles), and [29] (full circles)

where the parameters A_Y, B_Y, $\sqrt{s_0}$ are given in Table 1 and $\sqrt{s_0} = 1.6861\ GeV$.

The currently available experimental information (see Fig. 4) concerning the angular distribution of the outgoing kaons in the $\gamma p \to K^+\Lambda$ reaction in the photon energy range of interest can be fitted as:

Table 1. Parameters in the approximation of the partial cross sections for the production of K^+ mesons in γN collisions

Reaction	A_Y,$\mu b \cdot GeV$	B_Y, GeV^2	$\sqrt{s_0}$,GeV
$\gamma + p \to K^+ + \Lambda$	0.6343	0.0151	1.6093
$\gamma + n \to K^+ + \Sigma^-$	0.4562	0.0236	1.6909

$$\frac{d\sigma_{\gamma p\to K^+\Lambda}(s)}{d\overset{*}{\Omega}} = [1 + A_1(\sqrt{s})\cos\Theta_{K^+}]\frac{\sigma_{\gamma p\to K^+\Lambda}(\sqrt{s})}{4\pi}. \tag{14}$$

Here, Θ_{K^+} is the K^+ production angle in the c.m.s., the quantity $\sigma_{\gamma p\to K^+\Lambda}$ is defined above by the (12) and the parameter A_1 is given by:

$$A_1(\sqrt{s}) = \begin{cases} 0.928\left(\frac{\sqrt{s}-\sqrt{s_0}}{\mathrm{GeV}}\right)^{0.137} & \text{for } \sqrt{s_0} < \sqrt{s} \le 1.7372\,\mathrm{GeV} \\ 2.485\left(\frac{\sqrt{s}-\sqrt{s_0}}{\mathrm{GeV}}\right)^{0.616} & \text{for } 1.7372\,\mathrm{GeV} < \sqrt{s} \le 1.8375\,\mathrm{GeV} \\ 1 & \text{for } \sqrt{s} > 1.8375\,\mathrm{GeV}. \end{cases} \tag{15}$$

In our calculations, the angular distributions $d\sigma_{\gamma p\to K^+\Sigma^0}/d\overset{*}{\Omega}$ and $d\sigma_{\gamma n\to K^+\Sigma^-}/d\overset{*}{\Omega}$ were assumed to be isotropic [26].

To examine the influence of the uncertainties in the total cross section $\sigma_{\gamma p\to K^+\Lambda}$ for K^+ production via the dominant elementary process $\gamma p \to K^+\Lambda$ at subthreshold incident energies on the K^+ yield from nuclear targets, we will also use in our calculations the following parametrization of $\sigma_{\gamma p\to K^+\Lambda}$:

$$\sigma_{\gamma p\to K^+\Lambda}(\sqrt{s}) = \begin{cases} 3.60\left(\frac{\sqrt{s}-\sqrt{s_0}}{\mathrm{GeV}}\right)^{0.2275}\ [\mu\mathrm{b}] & \text{for } \sqrt{s_0} < \sqrt{s} \le 1.6204\,\mathrm{GeV} \\ 1.29\ [\mu\mathrm{b}] & \text{for } \sqrt{s} > 1.6204\,\mathrm{GeV}. \end{cases} \tag{16}$$

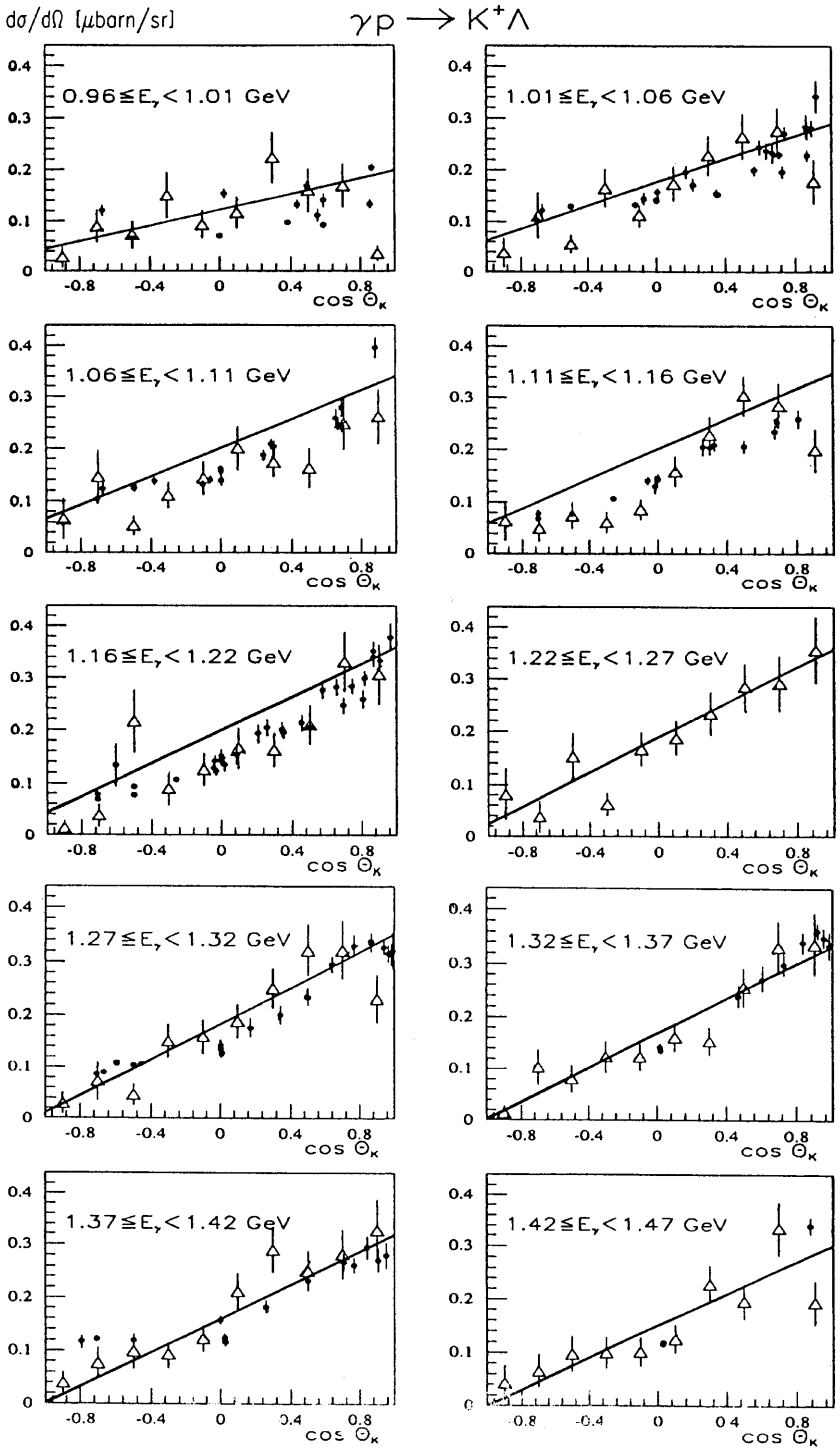

Fig. 4. Differential cross section for the reaction $\gamma p \to K^+\Lambda$. The solid line is calculation by (14), (15). Data are from [26]

It is shown by the dotted line in Fig. 1. A choice of the approximation of the total cross section $\sigma_{\gamma p\to K^+\Lambda}$ in the form (16) has been motivated by the fact that in the threshold energy region ($E_\gamma < 0.93\ GeV$) it practically coincides with the prediction for this cross section obtained in [30] within the pseudovector coupling description of the $KN\Lambda$ interaction with the value of coupling constant $g_{KN\Lambda}/\sqrt{4\pi} = -2.0$ settled close to the value calculated in [31] using the QCD sum rule method. Whereas at higher beam energies ($E_\gamma > 0.93\ GeV$) it reproduces also reasonably well the available data.

Before going to the next step, we discuss now the nucleon spectral function needed for our calculations. The nucleon spectral function, $P(\mathbf{p}_t, E)$, which represents the probability to find in the nucleus a nucleon with momentum $\mathbf{p}_t$ and removal (binding) energy E, is a crucial point in the evaluation of the subthreshold production of any particles on a nuclear target. When we consider the

ground–state NN correlations, which are generated by the short–range and tensor parts of realistic NN interaction, the spectral function $P(\mathbf{p}_t, E)$ can be represented in the following form [32, 33]:

$$P(\mathbf{p}_t, E) = P_0(\mathbf{p}_t, E) + P_1(\mathbf{p}_t, E), \tag{17}$$

where P_0 includes the ground and one–hole states of the residual $(A-1)$ nucleon system and P_1 more complex configurations (mainly 1p–2h states) that arise from the 2p–2h excited states generated in the ground state of the target nucleus by NN correlations. Before considering the specific expressions for functions P_0 and P_1, let us recall several important quantities which are related to the nucleon spectral function, namely [32, 33]:
the internal nucleon momentum distribution

$$\begin{aligned} n(\mathbf{p}_t) &= \int P(\mathbf{p}_t, E)dE \\ &= \int P_0(\mathbf{p}_t, E)dE + \int P_1(\mathbf{p}_t, E)dE \\ &= n_0(\mathbf{p}_t) + n_1(\mathbf{p}_t), \end{aligned} \tag{18}$$

the mean nucleon kinetic energy

$$\begin{aligned} < T > &= \int\int \frac{p_t^2}{2m_N} P(\mathbf{p}_t, E)d\mathbf{p}_t dE \\ &= \int \frac{p_t^2}{2m_N} n(\mathbf{p}_t)d\mathbf{p}_t, \end{aligned} \tag{19}$$

and the mean nucleon removal energy

$$< E >= \int\int EP(\mathbf{p}_t, E)d\mathbf{p}_t dE. \tag{20}$$

The last two quantities are related to the total binding energy per nucleon ϵ_A by the following energy sum rule (the Koltun sum rule [34]):

$$\epsilon_A = \frac{1}{2}\left(\frac{A-2}{A-1} < T > - < E >\right), \tag{21}$$

if the nuclear hamiltonian contains only two–body density–independent forces. The quantities ϵ_A and $n(\mathbf{p}_t)$ have been calculated [32, 33] for different nuclear systems ranging from light nuclei to infinite nuclear matter within the framework of many–body approaches with realistic NN interactions, so that the theoretical values of $< T >$ and $< E >$ for various nuclei are known presently [32, 33].

In calculating the cross sections for kaon production in γH^2 interactions, we have used for the nucleon spectral function $P(\mathbf{p}_t, E)$ the following expression [33]:

$$P(\mathbf{p}_t, E) = n_d(\mathbf{p}_t)\delta(E - |\epsilon_d|), \tag{22}$$

where $n_d(\mathbf{p}_t)$ is the nucleon momentum distribution in the deuteron and $|\epsilon_d| = 2.226\ MeV$ is the deuteron binding energy. The momentum distribution $n_d(\mathbf{p}_t)$ has been calculated in [33] using the Paris potential [35, 36] and the results of calculations have been parametrized as follows:

$$n_d(\mathbf{p}_t) = \frac{1}{4\pi}\sum_{i=1}^{3} A_i \frac{\exp\left(-B_i p_t^2\right)}{\left(1 + C_i p_t^2\right)^2}. \tag{23}$$

Table 2. Values of the parameters A_i, B_i and C_i appearing in the parametrization (23) of the nucleon momentum distribution in the deuteron

i	A_i, fm^3	$B_i,\ fm^2$	C_i, fm^2
1	157.4	1.24	18.3
2	0.234	1.27	
3	0.00623	0.22	

The values of the parameters appearing in (23) are given in Table 2.

It can be easily obtained that in case of the deuteron the off–shell energy E_t of the struck target nucleon given by (7) has the following simple form:

$$E_t = M_d - \sqrt{(-\mathbf{p}_t)^2 + m_N^2}. \tag{24}$$

Consider now the quantity $P(\mathbf{p}_t, E)$ for C^{12} and Pb^{208} target nuclei. For K^+ production calculations in the case of C^{12} and Pb^{208} target nuclei reported here we have employed for the single–particle (uncorrelated) part $P_0(\mathbf{p}_t, E)$ of the nucleon spectral function the following relation [10]:

$$P_0(\mathbf{p}_t, E) = \begin{cases} S_0 P^{(SM)}(\mathbf{p}_t, E) \text{ for } C^{12}, \\ S_0 P^{(FG)}(\mathbf{p}_t, E) \text{ for } Pb^{208}. \end{cases} \tag{25}$$

Here, $P^{(SM)}(\mathbf{p}_t, E)$ and $P^{(FG)}(\mathbf{p}_t, E)$ are the harmonic oscillator and Fermi–gas model spectral functions; the parameter $S_0 = 0.8$ [32, 33] takes into account the depletion of states below the Fermi sea due to the NN correlations. According to [10], one has [2]

$$\begin{aligned} P^{(SM)}(\mathbf{p}_t, E) = &\frac{4}{A} n_{1s}(\mathbf{p}_t)\delta(E - |\epsilon_{1s}|) \\ &+ \left(\frac{A-4}{A}\right) n_{1p}(\mathbf{p}_t)\delta(E - |\epsilon_{1p}|), \end{aligned} \tag{26}$$

where the s– and p–shell nucleon momentum distributions $n_{1s}(\mathbf{p}_t)$ and $n_{1p}(\mathbf{p}_t)$ are:

$$\begin{aligned} n_{1s}(\mathbf{p}_t) &= (b_0/\pi)^{3/2} \exp\left(-b_0 p_t^2\right), \\ n_{1p}(\mathbf{p}_t) &= \frac{2}{3}(b_0/\pi)^{3/2} b_0 p_t^2 \exp\left(-b_0 p_t^2\right) \end{aligned} \tag{27}$$

($b_0 = 68.5(\mathrm{GeV/c})^{-2}$) and binding energies of $|\epsilon_{1s}| = 34$ and $|\epsilon_{1p}| = 16\ MeV$ for the s and p shells, respectively, were used. The expression for $P^{(FG)}(\mathbf{p}_t, E)$ is [38]:

$$P^{(FG)}(\mathbf{p}_t, E) = \frac{1}{\frac{4}{3}\pi p_F^3}\theta(p_F - p_t)\delta(E - |\epsilon_{p_t}|), \tag{28}$$

[2] It should be pointed out that the use of Gaussian functions for the s– and p–shell nucleon removal energy distributions for C^{12} target nuclei in line with [37] in calculating the inclusive cross sections we are interested in, as showed our calculations, leads to the results which are sufficiently close to those obtained with the spectral function in the δ–function form (26).

where $\theta(x) = (x + |x|)/2|x|$, $\epsilon_{p_t} = (p_t^2/2m_N) + U_0$ (m_N is the rest mass of a nucleon), and the constants p_F, U_0 ($p_F^2/2m_N = 30.5\ MeV$, $U_0 = -50.7\ MeV$) for Pb^{208} were fixed requiring $< T >= 38.2\ MeV$, $< E >= 53.7\ MeV$ [33]. Here the mean kinetic $< T >$ and removal $< E >$ energies were calculated (see, formulas, (17)–(20), (25), (28)) according to the following expressions:

$$< T > = S_0 < T >_{FG} + < T >_1, \qquad (29)$$
$$< E > = S_0 < E >_{FG} + < E >_1,$$

where

$$< T >_{FG} = \frac{3}{5}\frac{p_F^2}{2m_N},\ < E >_{FG} = -(U_0 + < T >_{FG});$$
$$< T >_1 = \int \frac{p_t^2}{2m_N} n_1(\mathbf{p}_t) d\mathbf{p}_t,$$
$$< E >_1 = \int\int E P_1(\mathbf{p}_t, E) d\mathbf{p}_t dE \qquad (30)$$

and the spectral function $P_1(\mathbf{p}_t, E)$ is given below.

Let us focus now on the high momentum and high removal energy part (correlated part) $P_1(\mathbf{p}_t, E)$ of the nucleon spectral function. As was shown in [33], function $P_1(\mathbf{p}_t, E)$ can be expressed as a convolution integral of the momentum distributions describing the relative and center–of–mass motions of a correlated NN pair in the nuclear medium. An inspection of the convolution formula (53) from [33] for the spectral function $P_1(\mathbf{p}_t, E)$ leads to the following simple analytical expression for the $P_1(\mathbf{p}_t, E)$ (see, also, [10]):

$$P_1(\mathbf{p}_t, E) = a_1 n_1(\mathbf{p}_t)$$
$$\times \exp\left\{ -3[(A-2)/(A-1)]m_N \right.$$
$$\left. \times \left[\sqrt{E - E_{thr}} - \sqrt{E_1(p_t) - E_{thr}}\right]^2 / < p_{cm}^2 > \right\}, \qquad (31)$$

where

$$a_1 = \frac{3[(A-2)/(A-1)]m_N}{\left\{e^{-\alpha_0^2} + \alpha_0\sqrt{\pi}\,[1 + erf(\alpha_0)]\right\} < p_{cm}^2 >}, \qquad (32)$$

$$\alpha_0 = \frac{p_t}{(< p_{cm}^2 >)^{1/2}} \sqrt{\frac{3}{2}\left(\frac{A-2}{A-1}\right)^2 \left[1 - \left(\frac{A-1}{A-2}\right)\gamma\right]}, \qquad (33)$$

$$erf(x) = \frac{2}{\sqrt{\pi}} \int_0^x e^{-t^2} dt,$$

$$E_1(p_t) = E_{thr} + \left(\frac{A-2}{A-1}\right)\frac{p_t^2}{2m_N}\left[1 - \left(\frac{A-1}{A-2}\right)\gamma\right],$$
$$\gamma = \frac{< p_{cm}^2 >}{< p_{rel}^2 >}. \qquad (34)$$

Here, a_1 is a proper normalization constant (such that $\int_{E_{thr}}^{\infty} P_1(\mathbf{p}_t, E) dE = n_1(\mathbf{p}_t)$); $E_{thr} = M_{A-2} + 2m_N - M_A$ is the two–particle break–up threshold (E_{thr} is equal to 14 and 25 MeV for Pb^{208} and C^{12} target nuclei, respectively); $< p_{cm}^2 >$ and $< p_{rel}^2 >$ are the mean–square momenta associated with the low and high momentum parts of the momentum distribution describing the center–of–mass motion of a correlated NN pair and the momentum distribution describing the relative motion of this pair, respectively. In our calculations of the K^+ production cross sections on the C^{12} and Pb^{208} target nuclei we have used the values $< p_{cm}^2 >= 1.5 fm^{-2}$ for C^{12}, $< p_{cm}^2 >= 1.8 fm^{-2}$ for Pb^{208} and $< p_{rel}^2 >= 7.5 fm^{-2}$ [33] both for C^{12} and for Pb^{208}. The many–body momentum distribution $n_1(\mathbf{p}_t)$ for C^{12} has been presented in [32]. Taking into account the corresponding normalization of $n_1(\mathbf{p}_t)$ ($\int n_1(\mathbf{p}_t) d\mathbf{p}_t = S_1 = 1 - S_0 = 0.2$), it can be parametrized as follows [10]:

$$n_1(\mathbf{p}_t) = \frac{S_1}{(2\pi)^{3/2}(1 + \alpha_1)}$$
$$\times \left[\frac{1}{\sigma_1^3}\exp\left(-p_t^2/2\sigma_1^2\right) + \frac{\alpha_1}{\sigma_2^3}\exp\left(-p_t^2/2\sigma_2^2\right)\right], \qquad (35)$$

where $\sigma_1^2 = 0.162 fm^{-2}$, $\sigma_2^2 = 2.50 fm^{-2}$ and $\alpha_1 = 2.78$. This momentum distribution has been also employed in the case of Pb^{208} target nucleus [33].

Now let us perform an averaging of the $\gamma N \to K^+ Y$ inclusive invariant differential cross section (8) over the Fermi motion of the nucleons in the nucleus using the properties of the energy conserving Dirac δ–function. The integration in (5) over the angle ϑ between $\mathbf{p}_t$ and $\mathbf{Q}$ yields (see, also, [39, 40]):

$$\left\langle E_{K^+}\frac{d\sigma_{\gamma N \to K^+ Y}(\mathbf{p}_\gamma, \mathbf{p}_{K^+})}{d\mathbf{p}_{K^+}}\right\rangle =$$
$$\frac{\pi}{Q}\int_{E_{min}}^{E_{max}(Q,\omega)} dE \int_{p_t^{min}(Q,\omega,E)}^{p_t^{max}(Q,\omega,E)} p_t dp_t P(p_t, E)$$
$$\times \int_0^{2\pi} d\varphi \frac{1}{I_2[s(x_0,\varphi,E), m_Y, m_K]} \frac{d\sigma_{\gamma N \to K^+ Y}[s(x_0,\varphi,E)]}{d\overset{*}{\Omega}}, \qquad (36)$$

where

$$E_{min} = M_{A-1} + m_N - M_A,$$
$$E_{max} = E_{min} + \Delta_x;$$
$$\Delta_x = M_x - (M_{A-1} + m_Y),$$
$$M_x = [(\omega + M_A)^2 - Q^2]^{1/2}. \qquad (37)$$

The values of $p_t^{min}(Q, \omega, E)$ and $p_t^{max}(Q, \omega, E)$ are determined by the constraint $-1 \le \cos\vartheta \le 1$, with $\cos\vartheta$ given by the energy conservation

$$\omega + M_A = \sqrt{m_Y^2 + Q^2 + p_t^2 + 2Qp_t\cos\vartheta}$$
$$+\sqrt{(M_A - m_N + E)^2 + p_t^2}, \qquad (38)$$

and can be expressed as:

$$p_t^{min}(Q,\omega,E) = \alpha|p_t^{cm} - \beta E_{A-1}^{cm}|, \quad (39)$$

$$p_t^{max}(Q,\omega,E) = \alpha(p_t^{cm} + \beta E_{A-1}^{cm}), \quad (40)$$

where

$$E_{A-1}^{cm} = \sqrt{M_{A-1}^{*2} + (p_t^{cm})^2},$$
$$p_t^{cm} = \frac{1}{2M_x}\lambda(M_x^2, M_{A-1}^{*2}, m_Y^2),$$
$$M_{A-1}^{*} = M_A - m_N + E \quad (41)$$

and

$$\beta = Q/(\omega+M_A),\ \alpha = (1-\beta^2)^{-1/2} = (\omega+M_A)/M_x. \quad (42)$$

In (36)

$$s(x,\varphi,E) = (E_\gamma + E_t)^2 - p_\gamma^2 - p_t^2 - 2p_\gamma p_t \cdot (\cos\vartheta_{\mathbf{Q}}\cdot x + \sin\vartheta_{\mathbf{Q}}\cdot\sqrt{1-x^2}\cos\varphi), \quad (43)$$

$$x_0 = \left[(\omega+E_t)^2 - m_Y^2 - Q^2 - p_t^2\right]/(2Qp_t), \quad (44)$$

where

$$\cos\vartheta_{\mathbf{Q}} = \mathbf{p}_\gamma\mathbf{Q}/(p_\gamma Q),\ \sin\vartheta_{\mathbf{Q}} = \sqrt{1-\cos^2\vartheta_{\mathbf{Q}}}. \quad (45)$$

Because the nucleon spectral function $P(p_t,E)$ is a rapidly decreasing function of p_t and E, already for moderate values of the momentum transfer Q the quantities E_{max} and p_t^{max} can be safely replaced, as showed our calculations, by infinity. Therefore, the Q dependence of the momentum–energy–averaged differential cross section (36) will be essentially governed by the Q dependence of p_t^{min} (39). The latter is determined from the energy conservation (cf. (38))

$$\omega + M_A = \sqrt{m_Y^2 + (Q \pm p_t^{min})^2} + \sqrt{M_{A-1}^{*2} + (p_t^{min})^2}. \quad (46)$$

The positive and the negative signs in front of p_t^{min} in (46) correspond to $\omega > \omega_0$ and to $\omega < \omega_0$, respectively, with $\omega_0 = (m_Y^2 + Q^2)^{1/2} + M_{A-1}^{*} - M_A$. The foregoing leads, as is easy to see, to the conclusion that $x_0\Big|_{p_t=p_t^{min}} = +1$ for $\omega > \omega_0$ and $x_0\Big|_{p_t=p_t^{min}} = -1$ for $\omega < \omega_0$.

Let us discuss now the results of our calculations in the framework of the approach outlined above.

3 Results

Figure 5 shows a comparison of the calculated differential cross sections for the production of K^+ mesons at the laboratory angles of $10^0 \le \theta_{K^+} \le 40^0$ from primary $\gamma N \to K^+ Y$ channels with the experimental data [18] for $\gamma + C^{12} \to K^+ + X$ reaction at the various bombarding energies. The differential cross sections under consideration

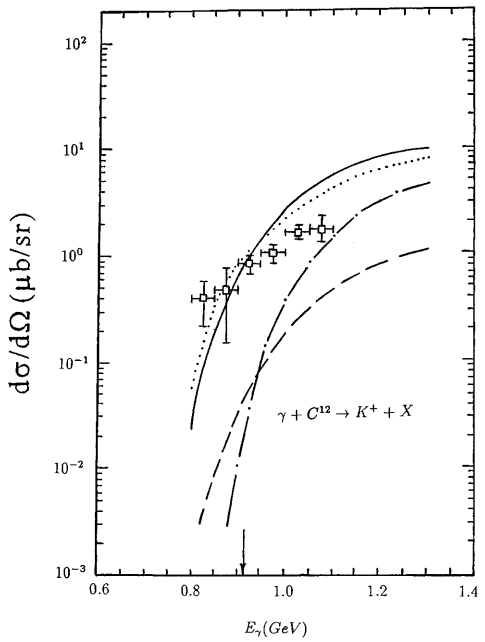

Fig. 5. Differential cross sections for K^+ production in $\gamma+C^{12}$ reactions in the angular domain $10^0 \le \theta_{K^+} \le 40^0$ in the lab system as functions of the laboratory energy of the photon. The experimental data (open squares) are from [18]. The curves are our calculation. The solid and dot–dashed lines are calculations by (47) with the total nucleon spectral function for primary production processes (1)–(3) and (2), (3), respectively. The parametrizations (12), (13) for the total cross sections of the subprocesses (1)–(3) were used in the above calculations. The dashed line denotes the same as solid line, but it is supposed that the total nucleon spectral function given by (17), (25) and (31) is replaced by its correlated part (31). The dotted line denotes the same as solid line, but it is supposed that the total cross section of the subprocess (1) given by (12) is replaced by the parametrization (16). The arrow indicates the threshold for the reaction $\gamma p \to K^+\Lambda$ occuring on a free proton

have been calculated according to the following expression:

$$\frac{d\sigma^{(prim)}_{\gamma A\to K^+X}(\mathbf{p}_\gamma)}{d\mathbf{\Omega}_{K^+}} = \frac{1}{[\cos(10^0) - \cos(40^0)]} \times \int_{10^0}^{40^0} \sin\theta_{K^+} d\theta_{K^+} \int_0^{p^{lim}_{K^+}(\theta_{K^+})} dp_{K^+} \frac{d^2\sigma^{(prim)}_{\gamma A\to K^+X}(\mathbf{p}_\gamma)}{dp_{K^+}d\mathbf{\Omega}_{K^+}}, \quad (47)$$

where

$$p^{lim}_{K^+}(\theta_{K^+}) = \frac{[\beta_A p_\gamma\cos\theta_{K^+} + (E_\gamma+M_A)\sqrt{\beta_A^2 - 4m_K^2(s_A + p_\gamma^2\sin^2\theta_{K^+})}]}{2(s_A + p_\gamma^2\sin^2\theta_{K^+})}; \quad (48)$$

$$\beta_A = s_A + m_K^2 - (M_{A-1} + m_Y)^2,$$
$$s_A = (E_\gamma + M_A)^2 - p_\gamma^2. \quad (49)$$

Here, $p^{lim}_{K^+}(\theta_{K^+})$ is the kinematical limit for kaon production at the lab angle θ_{K^+} from photon–nucleus interactions. The double differential cross section $d^2\sigma^{(prim)}_{\gamma A\to K^+X}(\mathbf{p}_\gamma)/dp_{K^+}d\mathbf{\Omega}_{K^+}$ entering into the (47) is defined above by the formulas (4), (5) and (36). The minimum value of the removal energy E_{min} (see, (37)) in the calculations was taken to be 15.5 MeV for C^{12} [41]. One can see that:

1) the contributions to the K^+ production from the primary reaction channels (1) and (2), (3) with Λ and Σ particles in the final states are comparable at bombarding energies $E_\gamma \geq 1.2$ GeV, whereas at lower incident energies the primary production process (1) is essentially more important than (2) and (3);
2) the kaon yield from the one–step K^+ production mechanism is entirely governed by the single–particle part $P_0(\mathbf{p}_t, E)$ of the nucleon spectral function at all considered beam energies (0.8 $GeV \leq E_\gamma \leq 1.3$ GeV), what makes difficult to extract the information on the high momentum and high removal energy components within the C^{12} target nucleus from the first kaon photoproduction experiment [18];
3) while our calculations for the one–step reaction channels (1)–(3) carried out under two assumptions about the total cross section of the subprocess (1) following from formulas (12) (solid line) and (16) (dotted line) reproduce reasonably well the experimental data [18] in the energy region of interest, they nevertheless provide different energy dependence of the excitation function as compared to the data, what might be due to possible in–medium modifications of the elementary $\gamma N \to K^+Y$ reactions discarded in the present work;
4) the experimental data are better described by our first chance collision model when the parametrization (16) for the total cross section of the elementary process $\gamma p \to K^+\Lambda$ has been employed, what indicates the need for high quality kaon photoproduction data both on the proton and nuclear targets at considered beam energies from the future experiments [19, 20, 42] to reliably test the spectral function approach presented in this study as well as to deeply elucidate the underlying mechanism of subthreshold and near threshold kaon photoproduction and possible modifications of the elementary photon–nucleon interaction in the nuclear medium.

In Fig. 6 we show the predictions of the above model for the differential cross sections for the production of K^+ mesons from primary $\gamma N \to K^+Y$ reaction channels at the laboratory angles of $10^0 \leq \theta_{K^+} \leq 40^0$ in the interaction of different energy photons with the deuterons. Inspection of Figs. 5 and 6 tells us that the K^+ differential cross sections on C^{12} and H^2 show charge number dependence approximately proportional to Z in the threshold region. This simply indicates that the results under consideration are insensitive to the details of the low momentum part of the internal nucleon momentum distribution.

Figure 7 presents the results of our calculations by (4), (5) and (36) for the double differential cross sections for the production of K^+ mesons at an angle [3] of 10^0 in the interaction of photons with energies of 0.8, 0.9 and 1.3 GeV with C^{12} nuclei. It is seen that:

1) the calculated kaon momentum spectra reveal characteristic features of quasifree production (a singly peaked structure the width of which reflects Fermi

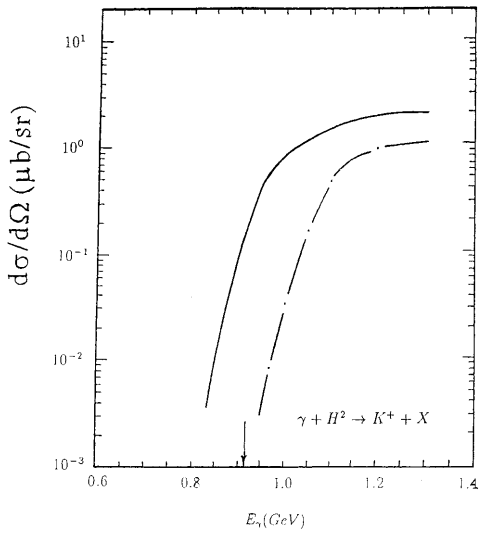

Fig. 6. Differential cross sections for K^+ production in $\gamma + H^2$ reactions in the angular domain $10^0 \leq \theta_{K^+} \leq 40^0$ in the lab system as functions of the laboratory energy of the photon. The notation is identical to that in Fig. 5

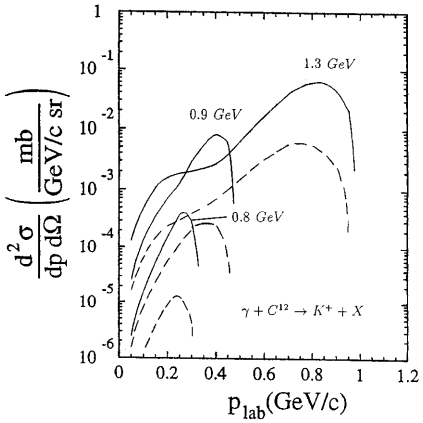

Fig. 7. Double differential cross sections for the production of K^+ mesons at an angle of 10^0 in the interaction of 0.8, 0.9 and 1.3 GeV photons with the C^{12} nuclei as functions of kaon momentum. The solid and dashed lines represent our calculations by (4), (5) and (36) for primary production processes (1)–(3) with the use of total nucleon spectral function and its correlated part, respectively, and correspond from the top to the bottom 1.3, 0.9 and 0.8 GeV incident energy. The parametrizations (12), (13) for the total cross sections of the subprocesses (1)–(3) were used in the above calculations

[3] A choice of this angle has been particularly motivated by the fact that in the threshold energy region kaons are mainly emitted in forward directions.

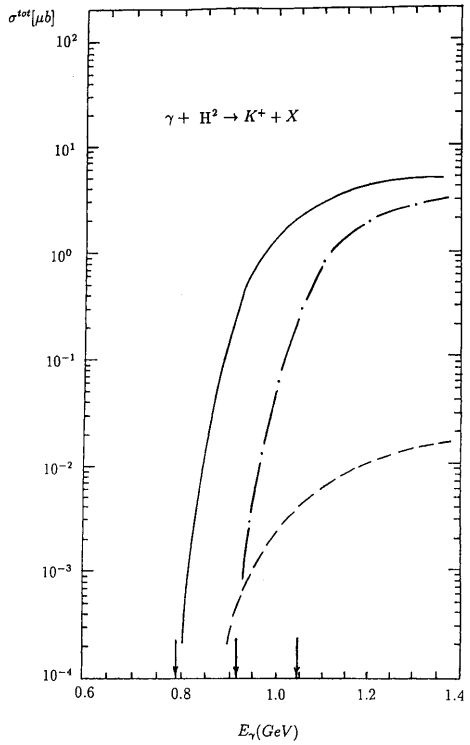

Fig. 8. Total cross section for K^+ production in $\gamma + H^2$ reactions as a function of the laboratory energy of the photon. The solid and dot–dashed lines are calculations with the "total" nucleon spectral function for primary production processes (1)–(3) and (2), (3), respectively. The dashed line denotes the same as solid line, but it is supposed that the "total" nucleon spectral function given by (22) and (23) is replaced by the "model" nucleon spectral function in which only the internal nucleon momenta greater than 0.5 GeV/c are taken into account. The parametrizations (12), (13) for the total cross sections of the subprocesses (1)–(3) were used in the above calculations. The arrows indicate the thresholds for the reactions $\gamma p \to K^+\Sigma^0$, $\gamma p \to K^+\Lambda$ occuring on a free proton and the absolute production threshold

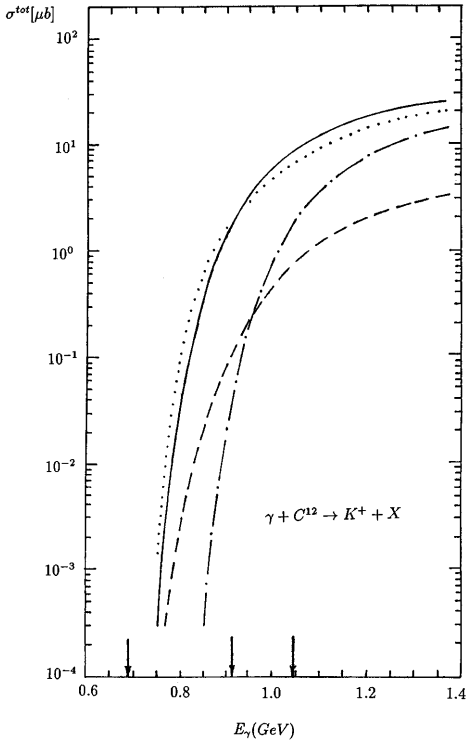

Fig. 9. Total cross section for K^+ production in $\gamma + C^{12}$ reactions as a function of the laboratory energy of the photon. The solid and dot–dashed lines are calculations with the total nucleon spectral function for primary production processes (1)–(3) and (2), (3), respectively. The parametrizations (12), (13) for the total cross sections of the subprocesses (1)–(3) were used in the above calculations. The dashed line denotes the same as solid line, but it is supposed that the total nucleon spectral function given by (17), (25) and (31) is replaced by its correlated part (31). The dotted line denotes the same as solid line, but it is supposed that the total cross section of the subprocess (1) given by (12) is replaced by the parametrization (16). The arrows indicate the thresholds for the reactions $\gamma p \to K^+\Sigma^0$, $\gamma p \to K^+\Lambda$ occuring on a free proton and the absolute production threshold

broadening, an asymmetric spectral shape) even at subthreshold incident energies;

2) the main contribution to the K^+ production both at subthreshold and above the free γN threshold beam energies considered here comes from the use of the uncorrelated part[4] $P_0(\mathbf{p}_t, E)$ of the nucleon spectral function in the calculation of the corresponding momentum–energy–averaged differential cross sections for kaon production, what makes rather difficult to extract the information on the correlated part of the nucleon spectral function even through analysis of the experimental double differential cross sections for K^+ production at adopted photon energies ($E_\gamma \geq 0.8\ GeV$).

The total cross section for K^+ production in $\gamma + H^2$ reactions calculated according to (4) is shown in Fig. 8 as a function of the laboratory photon energy E_γ. It is seen that the kaon yield from the direct K^+ production processes (1)–(3) is entirely governed by the low momentum part ($p_t < 0.5\ GeV/c$) of the deuteron momentum distribution at considered bombarding energies (at beam energies between the absolute reaction threshold and 1.4 GeV), what makes difficult to test the high momentum tail of $n_d(\mathbf{p}_t)$ from the measurement of the primary–photon energy dependence of the total cross section for K^+ production in γH^2 collisions even in the far subthreshold region ($E_\gamma \sim 0.8\ GeV$). One can also see that the contributions to the K^+ production from primary reaction channels (1) and (2), (3) with Λ and Σ particles in the final states are comparable at beam energies $E_\gamma \geq 1.2\ GeV$, whereas at lower incident energies the primary production process (1) is more important than (2) and (3). This is consistent with our previous findings of Figs. 5 and 6.

[4] Compare to the analogous conclusion drawn from the analysis of the kaon differential cross sections presented in Figure 5.

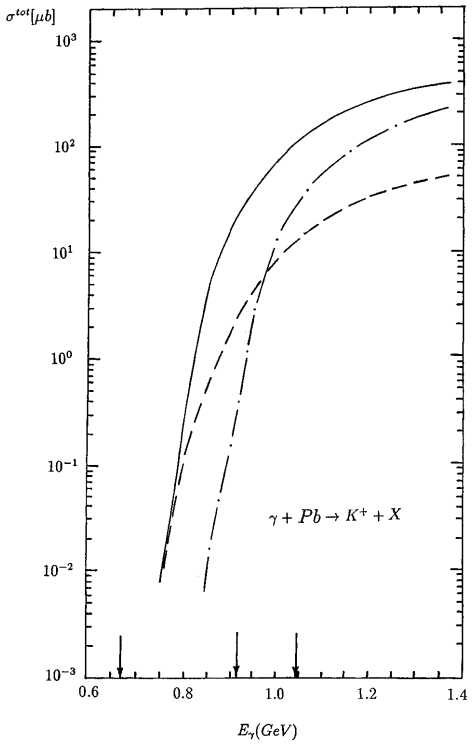

Fig. 10. Total cross section for K^+ production in $\gamma + Pb^{208}$ reactions as a function of the laboratory energy of the photon. The notation is identical to that in Fig. 9

Figures 9 and 10 present the results of similar calculations by (4) for the total cross sections for K^+ production in $\gamma + C^{12}$ and $\gamma + Pb^{208}$ reactions, respectively. It can be seen that in these cases the kaon yield from the one–step K^+ production mechanism is almost completely determined by the correlated part $P_1(\mathbf{p}_t, E)$ of the nucleon spectral function only in the vicinities of the absolute reaction thresholds (at bombarding energies of $E_\gamma \leq 0.75\ GeV$). This conclusion is in line with our findings inferred above (cf. Figs. 5 and 7) from the analysis of differential and double differential kaon production cross sections. The values of the total kaon production cross sections in the far subthreshold region ($E_\gamma \leq 0.75\ GeV$) are very small (in the range of 0.1–10 nb), but one should expect to measure these values on modern experimental facilities such as the CEBAF [19, 20], ELectron Stretcher Accelerator (ELSA) [26] and European Synchrotron Radiation Facility (ESRF) [29]. As in the preceding cases, the direct K^+ production processes (2), (3) play a minor role in kaon production in γA interactions at beam energies of $E_\gamma < 1.2\ GeV$. It is also seen from Fig. 9 that the extrapolations (12) and (16) of the elementary cross section for $\gamma p \to K^+\Lambda$ reaction to the threshold lead to different numerical predictions[5] for the respective kaon production cross sections in γC^{12} collisions in the energy region far below the lowest threshold (at incident energies of $E_\gamma \sim 0.75\ GeV$). Thus, to achieve a better understanding of the phenomenon of the deep subthreshold K^+ production in γA interactions it is important to measure the elementary cross section under consideration close to the threshold.

Kinematical considerations show that the two–step kaon production processes of the type $\gamma N \to MN$, $MN \to K^+Y$; $M = \{\pi, \eta\}$ may contribute to the (γ, K^+) reaction on nuclei at subthreshold incident energies. We have neglected in the present work the two–step kaon creation processes mentioned above in calculating the K^+ production cross sections from γA reactions, since the contribution from them to these cross sections is expected to be small in the bombarding energy range of our main interest ($E_\gamma \leq 0.8\ GeV$) where the intermediate pion and eta are produced, as showed our calculations, with energies at which secondary $MN \to K^+Y$ channels are energetically suppressed. Nevertheless, it would be interesting to carry out in the future a detailed study of subthreshold kaon production from the two–step processes under consideration.

Thus, our results demonstrate that it is difficult to distinguish the contribution to K^+ production in γA reactions from the high momentum and high removal energy part of the nucleon spectral function which is generated by ground–state two–nucleon short–range correlations inside the target nucleus with the measurements of the K^+ total and differential cross sections at subthreshold photon energies.

4 Conclusions

In this paper we have calculated the total and differential cross sections for K^+ production from $\gamma + H^2$, $\gamma + C^{12}$ and $\gamma + Pb^{208}$ reactions in the near threshold and subthreshold energy regimes by considering incoherent primary photon–nucleon production processes within the framework of the first collision model based on free elementary cross sections for kaon production and on the nucleon spectral function. The comparison of the results of our calculations with the existing experimental data [18] was made. It was shown that while our calculations reproduce reasonably well these data, they nevertheless provide different energy dependence of the excitation function as compared to the data. It was found also that in the case of $\gamma + H^2$ reaction the calculated K^+ production cross sections are completely determined by the low momentum part ($p_t < 0.5\ GeV/c$) of the deuteron momentum distribution. Whereas in the case of $\gamma + C^{12}$ and $\gamma + Pb^{208}$ reactions they are entirely governed by the correlated part of the nucleon spectral function only in the vicinities of the absolute reaction thresholds, what makes rather difficult to extract the information on the high momentum–energy component of the nucleon spectral function from the measurements of the total and differential cross sections for K^+ production in γA interactions at subthreshold photon energies.

The author would like to thank Yu.T. Kiselev and V.A. Sheinkman for interest in the work.

[5] The difference between these predictions is of order 5.

References

1. Koptev, V.P., Mikirtyhyants, S.M., Nesterov, M.M., Tarasov, N.A., Shcherbakov, G.V., Abrosimov, N.K., Volchenkov, V.A, Gridnev, A.B., Yeliseyev, V.A., Ivanov, E.M., Kruglov, S.P., Malov, Yu.A., Ryabov, G.A.: *ZhETF.* **94**, 1 (1988)
2. Shor, A., Perez-Mendez, V., Ganezer, K.: *Nucl. Phys.* **A514**, 717 (1990)
3. Cassing, W., Batko, G., Mosel, U., Niita, K., Schult, O., Wolf, Gy.: *Phys. Lett.* **238B**, 25 (1990)
4. Sibirtsev, A.A., Büscher, M.: *Z. Phys.* **A347**, 191 (1994)
5. Cassing, W., Demski, T., Jarczyk, L., Kamys, B., Rudy, Z., Schult, O.W.B., Strzalkowski, A.: *Z. Phys.* **A349**, 77 (1994)
6. Sibirtsev, A.: *Phys. Lett.* **359B**, 29 (1995)
7. Müller, H., Sistemich, K.: *Z. Phys.* **A344**, 197 (1992)
8. Debowski, M., Barth, R., Boivin, M., Le Bornec, Y., Cieslak, M., Comets, M.P., Courtat, P., Gacougnolle, R., Grosse, E., Kirchner, T., Martin, J.M., Miskowiec, D., Müntz, C., Schwab, E., Senger, P., Sturm, C., Tatischeff, B., Wagner, A., Walus, W., Willis, N., Wurzinger, R., Yonnet, J., Zghiche, A.: *Z. Phys.* **A356**, 313 (1996)
9. Sibirtsev, A., Cassing, W., Mosel, U.: *Z. Phys.* **A358**, 357 (1997)
10. Efremov, S.V., Paryev, E.Ya.: *Eur. Phys. J.* **A1**, 99 (1998)
11. Akindinov, A.V., Chumakov, M.M., Kiselev, Yu.T., Martemyanov, A.N., Mikhailov, K.R., Pozdnyakov, S.A., Sheinkman, V.A., Terekhov, Yu.V.: *APH N.S., Heavy Ion Physics* **4**, 325 (1996)
12. Kiselev, Yu.T., Firozabadi, M.M., Ushakov, V.I.:*Preprint ITEP* **56–96**, Moscow (1996)
13. Kopeliovich, B.Z., Niedermeier, F.: *Yad. Fiz.* **V.44**, 517 (1986)
14. Badala, A., Barbera, R., Bassi, M., Bonasera, A., Gulino, M., Librizzi, F., Mascali, A., Palmeri, A., Pappalardo, G.S., Riggi, F., Russo, A.C., Russo, G., Turrisi, R., Dunin, V., Ekstrom, C., Ericsson, G., Hoistad, B., Johansson, J., Johansson, T., Westerberg, L., Zlomaczhuk, J., Sibirtsev, A.: *Phys. Rev. Lett.* **80**, 4863 (1998)
15. Paryev, E.Ya.: *Eur. Phys. J.* **A5**, 307 (1999)
16. Efremov, S.V., Paryev, E.Ya.: *Z. Phys.* **A351**, 447 (1995)
17. Efremov, S.V., Paryev, E.Ya.: *Z. Phys.* **A354**, 219 (1996)
18. Yamazaki, H., Maeda, K., Asano, S., Emura, T., Endo, S., Ito, S., Itoh, H., Konno, O., Maruyama, K., Niwa, K., Sakaguchi, A., Suda, T., Sumi, Y., Takeya, M., Terasawa, T., Yamashita, H.: *Phys. Rev.* **C52**, R1157 (1995)
19. *CEBAF experiment* **91–014** (C.E. Hyde–Wright spokesman)
20. Mecking, B.A.: *Nucl. Phys.* **A639**, 559c (1998)
21. Kaplan, D.B., Nelson, A.E.: *Phys. Lett.* **175B**, 57 (1986); Nelson, A.E., Kaplan, D.B.: *Phys. Lett.* **192B**, 193 (1987)
22. Yamamoto, Y., Bando, H.: *Phys. Lett.* **214B**, 173 (1988)
23. Hjorth–Jensen, M., Polls, A., Ramos, A., Muther, H.: *Nucl.Phys.* **A605**, 458 (1996)
24. Li, G.Q., Ko, C.M.: *Phys. Rev.* **C54**, 1897 (1996)
25. Ciofi degli Atti, C., Simula, S.: *Phys. Lett.* **325B**, 276 (1994)
26. Bockhorst, M., Burbach, G., Burgwinkel, R., Empt, J., Guse, B., Haas, K.–M., Hannappel, J., Heinloth, K., Hey, T., Hoffmann–Rothe, P., Honscheid, K., Jahnen, T., Jakob, H.P., Jopen, N., Jungst, H., Kirch, U., Klein, F.–J., Kostrewa, D., Lindemann, L., Link, J., Manns, J., Menze, D., Merkel, H., Merkel, R., Neuerburg, W., Paul, E., Plotzke, R., Schenk, U., Schmidt, S., Scholmann, J., Schutz, P., Schultz–Coulon, H.–C., Schweitzer, M., Schwille, W.J., Tran, M.–Q., Umlauf, G., Vogl, W., Wedemeyer, R., Wehnes, F., Wiskirchen, J., Wolf, A.: *Z. Phys.* **C63**, 37 (1994)
27. ABBHHM Coll.: *Phys. Rev.* **188**, 2060 (1969)
28. Mart, T., Bennhold, C., Hyde–Wright, C.E.: *Phys. Rev.* **C51**, R1074 (1995)
29. David, J.C., Fayard, C., Lamot, G.H., Saghai, B.: *Phys. Rev.* **C53**, 2613 (1996)
30. Cheoun, M.K., Han, B.S., Yu, B.G., Cheon, Il–Tong: *Phys. Rev.* **C54**, 1811 (1996)
31. Choe, S., Cheoun, M.K., Lee, S.H.: *Phys. Rev.* **C53**, 1363 (1996)
32. Ciofi degli Atti, C., Liuti, S.: *Phys. Lett.* **225B**, 215 (1989)
33. Ciofi degli Atti, C., Simula, S.: *Phys. Rev.* **C53**, 1689 (1996)
34. Koltun, D.S.: *Phys. Rev.* **C9**, 484 (1974)
35. Lacombe, M., Loiseau, B., Richard, J.M., Mau, R.Vinh, Cote, J., Pires, P., de Tourreil, R.: *Phys. Rev.* **C21**, 861 (1980)
36. Lacombe, M., Loiseau, B., Mau, R.Vinh, Cote, J., Pires, P., de Tourreil, R.: *Phys. Lett.* **101B**, 139 (1981)
37. Hiramatsu, H., Kamae, T., Muramatsu, H., Nakamura, K., Izutsu, N., Watase, Y.: *Phys. Lett.* **44B**, 50 (1973)
38. Benhar, O., Pandharipande, V.R., Sick, I.: *Phys. Lett.* **410B**, 79 (1997)
39. Pace, E., Salme, G.: *Phys. Lett.* **110B**, 411 (1982)
40. Ciofi degli Atti, C., Pace, E., Salme, G.: *Phys. Rev.* **C43**, 1155 (1991)
41. Frullani, S., Mougey, J.: *Adv. Nucl. Phys.* **14**, 1 (1984)
42. Fujiwara, M.: *The APCTP Workshop on* **Strangeness Nuclear Physics (SNP'99)**. Seoul, Republic of Korea, February 19–22, 1999. Book of Abstracts, p.83